Bulletin of Engineering Geology and the Environment (2022) 81: 159
https://doi.org/10.1007/s10064-022-02651-w

ORIGINAL PAPER

# Effect of thermal treatment on the expansion characteristics of the diesel-contaminated soil and its mechanism

Yeyang Chun[1] · Jing Du[2] · Dong Zhou[1] · Zonghui Liu[1] · Tenglong Liang[1] · Jiawei Qin[1] · Jian Su[3]

Received: 8 July 2021 / Accepted: 9 March 2022 / Published online: 24 March 2022


## Abstract

Adopting the expansive soil in Nanning, China, as the pollution-free background soil, and 0# diesel as the petroleum hydrocarbon pollutant, the effect of thermal treatment on the expansion characteristics of contaminated soil by diesel was studied. X-ray diffraction (XRD), mercury intrusion porosimetry method (MIP), scanning electron microscopy (SEM), and gas chromatography-flame ionization detection (GC-FID) were adopted in a study of the effect mechanism. The results reveal that at a constant diesel content, the steady-state no-load expansion ratio (Steady ER) of the thermal treated diesel-contaminated expansive soil (TT-ES) decreases with increasing heating temperature, and the expansion time history curve changes from a three-stage shape to a straight-line shape. The XRD test results show that the content of illite, which determines the expansion characteristics of the TT-ES, has not changed during the thermal treatment and cannot be used to explain the decrease of expansion characteristics of TT-ES. However, the change of its crystal structure can have an impact on the expansion characteristics. Within the heating temperature range from 500 ~ 800 °C, the cation exchange capacity decreases, which reduces the hydration reaction of the TT-ES, thereby decreasing the Steady ER. Within the full heating temperature range, the soil structure affects the time history curve shape and the Steady ER. When the heating temperature remains constant, the larger the diesel fuel amount was, the lower Steady ER. Similarly, the decrease in cation exchange capacity due to the incorporation of diesel oil and the change of the soil structure reduce the Steady ER.

**Keywords** Thermal treatment · Diesel-contaminated expansive soil · Illite · Cation exchange capacity · Soil texture · Residual carbon

✉ Dong Zhou
zhd@gxu.edu.cn

Yeyang Chun
chunyeyangcyy@163.com

Jing Du
djsenate@163.com

Zonghui Liu
lzh8@gxu.edu.cn

Tenglong Liang
1410401002@st.gxu.edu.cn

Jiawei Qin
qinge1997888@163.com

Jian Su
nnsujian@163.com

[1] College of Civil Engineering and Architecture, Guangxi University, Nanning 530004, Guangxi, China

[2] Guangxi Transport Vocational and Technical College, Guangxi, Nanning 530023, China

[3] Guangxi Bossco Environmental Protection Technology Co., Ltd, Nanning 530004, China

## Introduction

In the process of exploration, mining, refining, processing, and transportation, oil often enters the soil in the form of oily wastewater, reservoir crude oil, and oily waste mud due to accidents (Kamnikar 2001; Zhang et al. 2012). Petroleum and petroleum hydrocarbons do not easily degrade and persist in soil, thereby threatening human health and the growth of animals and plants (Li et al. 2019). Petroleum hydrocarbons that remain in the soil for a long time can increase the human carcinogenic rate approximately 150 times (Bortey-Sam et al. 2014; Xiong and Wang 2021), produce acute and chronic symptoms, alter the state of the endocrine system, and increase the endpoint of genotoxicity (Pérez-Cadahía et al. 2006, 2007). Moreover, oil can invade the organs and tissues of animals, and even kill the animals living in the soil, such as earthworms (Gospodarek et al. 2019). The stomata and cell walls of plant tissues are blocked, the transpiration

rate and photosynthesis are reduced, and plant growth is inhibited, with plant death eventually occurring (Chaineau et al. 1997; Han et al. 2016; Pérez-Hernández et al. 2016). Therefore, the removal of petroleum and petroleum hydrocarbons from the soil is necessary.

Since most petroleum and petroleum hydrocarbons exhibit volatile and semi-volatile properties, heat treatment is usually implemented to remove and remediate petroleum- and petroleum hydrocarbon-contaminated soil (Vidonish et al. 2016). The thermal treatment technique promotes thermal desorption and pyrolysis of pollutants by heating contaminated soil and extracting these pollutants from soil (Ren et al. 2020). The most prominent feature of the thermal treatment technique is the application of a high temperature, and the maximum heating temperature can reach 800 °C (Merino and Bucalá 2007). Heat treatment affects the soil properties when cleaning and repairing contaminated soil using the high-temperature environment of manufacturing (Sun et al. 2020). For example, due to high temperature, changes in particle gradation (Roh et al. 2000; O'Brien et al. 2016) aggregate stability (Inbar et al. 2014; Badía-Villas et al. 2014) and mechanical properties (Gulgun 2011), etc.

Expansive soil is a common clay. It is a highly plastic clay that expands when absorbing water and shrinks when it loses water (Ali and Mohamed 2018). Its expansion and contraction characteristics can bring great harm, and this kind of harm often has repetitive and long-term potential (Okeke 2020). The immersion of petroleum or petroleum hydrocarbon and heat treatment can change its properties and have an important effect on the expansion characteristics (Magzoub et al. 2017; Bojnourdi et al. 2020). Moreover, however, there are few articles on the expansion characteristics and mechanism of expansive soil polluted by petroleum or petroleum hydrocarbon. It can provide a basis for the reuse of petroleum hydrocarbon contaminated soil after thermal treatment.

In this paper, Nanning expansive soil is adopted as the non-polluted background soil, diesel oil, is employed as a replacement for petroleum pollutants, and polluted soil is artificially prepared and thermally treated. Via the measurement of the no-load expansion rate of diesel-contaminated soil after thermal treatment, the effect of thermal treatment and diesel contamination on the expansion characteristics of expansive soil is determined. From the perspectives of clay minerals, cation exchange capacity, soil structure, and residual carbon, the effect mechanism of thermal treatment and diesel oil contamination on the expansion characteristics of TT-ES are studied and analyzed. It can provide a basis for the reuse of diesel contaminated soil after heat treatment.

## Materials and methods

### Experimental soil sample

The experimental soil was collected in a pasture near the bridgehead of the Buffalo Research Institute in Nanning city, Guangxi Province, at a soil depth of approximately 0.5 m, and the color of the expansive soil is off-white. The overlying soil layers above expansive soil include root soil (approximately 0.2 m thick) and red clay (approximately 0.25 m thick). The experimental soil was stored in sealed plastic bags and transported to the laboratory. The experimental soil was dried and crushed, and impurities were removed. The experimental soil was then passed through a 2-mm sieve and stored for later use. The basic physical properties of the expansive soil are listed in Table 1.

### Diesel oil

The diesel oil applied in the experiment is 0# diesel oil sold on the market in China. The color of the diesel oil is light green, the relative density is 0.856, and the viscosity coefficient is 3.95 mPa•s at 20 °C.

### Experimental design

Set 4 kinds of diesel content (0.0wt%, 2.0wt%, 4.0wt%, and 6.0wt%), 1 kind of moisture content (30%) and 1 kind of dry density (1.41 g•cm$^{-3}$), and 8 heating temperature nodes (100 °C, 200 °C, 300 °C, 400 °C, 500 °C, 600 °C, 700 °C, and 800 °C). For the convenience of description, the diesel content is numbered 0.0wt% → I, 2.0wt% → II, 4.0wt% → III, 6.0wt% → IV. The heating temperature number is 100 °C → 1#, 200 °C → 2#, 300 °C → 3#, 400 °C → 4#, 500 °C → 5#, 600 °C → 6#, 700 °C → 7#, 800 °C → 8#. $S_{III,1\#}$ represents the sample after the diesel content is 4.0wt% and the heating temperature is 100 °C and carried out a no-load and confined expansion experiment, mineral composition and content test (XRD analysis), exchangeable cation content test and micro-morphology test (SEM), and gas chromatography-flame ionization detection (GC-FID).

**Table 1** Basic physical properties of expansive soil

| Natural moisture content (%) | Natural density (g.cm$^{-3}$) | Specific gravity | Liquid limit (%) | Plastic limit (%) | Free expansion rate (%) |
|---|---|---|---|---|---|
| 32.8 | 1.84 | 2.73 | 75.3 | 26.7 | 59.0 |

The essence of the thermal treatment technique is to eliminate organic pollutants in soil (in this case diesel) through exposure to a high temperature to below the screening value (the screening value is 826 mg/kg in China). Therefore, the heating time in this article is based on whether the residual diesel amount in the TT-ES is lower than the standard screening value after thermal treatment. A soil sample with a diesel content of 6.0 wt% was treated at a heating temperature of 100 °C under different heating times, and the residual diesel content was measured. Test sampling points are shown in Fig. 1a. After a test heating time of 38 h, the measured value reached 697 mg/kg, which is lower than the standard screening value of 826 mg/kg (Wei and Wang 2020). To ensure a good removal effect, the heating time was extended by 2 h, and the heating time was thus set to 40 h in this paper.

## Experimental method

### Preparation of diesel-contaminated soil

To ensure a uniform distribution of distilled water and diesel in the soil samples, a layered sample preparation method was implemented to prepare soil samples with a water content of 30% and diesel contents of 0.0 wt%, 2.0 wt%, 4.0 wt%, and 6.0 wt%. Each prepared soil sample was sealed in a plastic bag and placed in a dark environment (Lee et al. 1998). During this period, the soil samples contained in sealed bags were rotated several times.

### Preparation of diesel-contaminated soil ring cutting specimens

The dry density was controlled at 1.41 g•cm$^{-3}$, and a ring knife sample with a size of ϕ61.8 × 20 mm was prepared via the one-time compression method. The prepared ring knife sample was stored in a sealed plastic bag and placed in a dark environment for storage.

Diesel-polluted soil thermal treatment experiment. In the experiment, a high-temperature muffle furnace was employed to simulate soil thermal treatment under the action of different heating temperatures. To avoid the influence of the bottom contact boundary on the soil sample during the heating process, the soil sample was placed on a high-temperature resistance stainless steel wire mesh during heat treatment, as shown in Fig. 1b. In the simulated heat treatment, a negative pressure of −0.1 kPa was maintained. During remediation, the ring cutting specimen experienced body shrinkage, as shown in Fig. 1c.

No-load confined expansion rate experiment. According to the guidelines of the People's Republic of China Geotechnical Test Method Standard (GB/T 50,123–2019), the no-load confined expansion rate experiment was performed (Wang et al. 2020). Since the ring cutting sample shrank and fractured to different degrees during the thermal treatment process, the gap between the ring cutter and TT-ES was filled to meet the requirements of the no-load confined expansion rate experiment. When filling the gap, the TT-ES was first sealed and enclosed in plastic wrap, the gap was then filled with several layers of hard polyvinyl chloride (PVC) plastic film of different thicknesses, and the remaining gap was finally filled with epoxy resin. A schematic diagram of the gap-filling process is shown in Fig. 2. It should be noted that the plastic film layers on the upper and lower bottom surfaces were removed during the no-load confined expansion rate experiment.

### Mineral composition and semi-quantitative analysis (XRD analysis)

The mineral composition and content are carried out in Zhongke Baitest Co., Ltd. During the test, the soil sample was mixed with 20% zinc oxide as an internal standard for semi-quantitative analysis of mineral composition. The test instrument is a RIGAKU D/max-2500v diffractometer, the

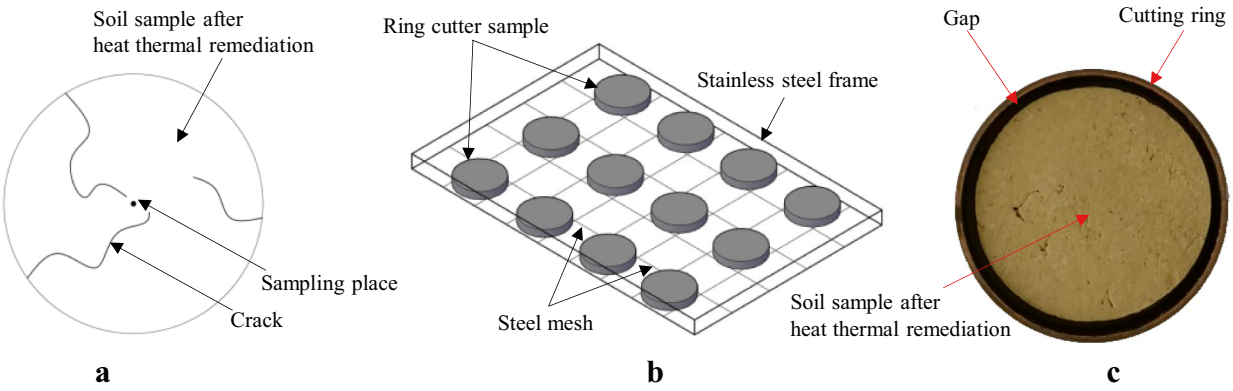


**Fig. 1** Test design and demonstration. (**a**) Schematic diagram of diesel residual sampling. (**b**) Layout of ring cutter sample for diesel contaminated expansive soil. (**c**) Sample drawing of ring cutter after thermal remediation. The picture is drawn with CAD and processed with PPT

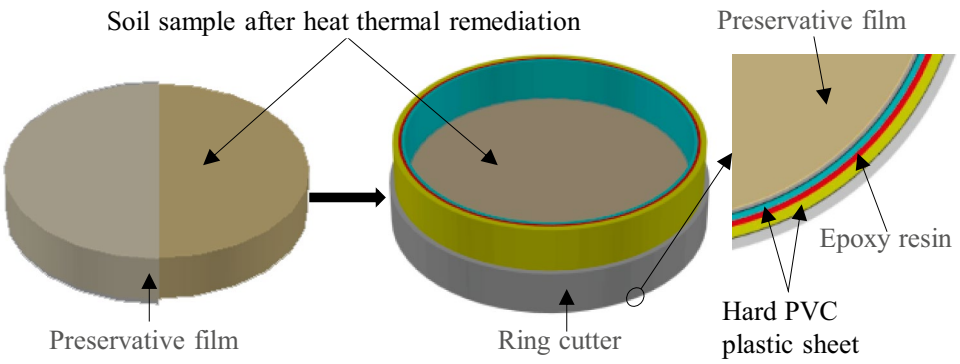


**Fig. 2** Schematic diagram of the gap. The picture is drawn with CAD and processed with PPT

CuK α radiation range is 3–90°, and the step length is 3°. TOPAS software was used to analyze the mineral composition (Lin and Cerato 2012; Hollanders et al. 2016).

The exchange cation capacity was tested at the Geological and Mineral Testing and Research Center of Guangxi Zhuang Autonomous Region.

The residual diesel content in the soil was tested by Guangxi Boce Testing Technology Service Co., Ltd (GC-FID).

The porosity of soil was tested in Guangzhou nano micro Testing Co., Ltd (MIP).

The microscopic morphology of soil particles was analyzed by scanning electron microscopy (S-3400 N) from Hitachi, Japan, and the test samples were prepared by freeze-drying method (Watabe et al. 2011). The specific method is: quickly put the cut soil block into liquid nitrogen (boiling point −196 °C) and freeze for 1 ~ 2 h, so that the moisture in the soil quickly condenses into non-expandable ice, and then vacuum at −50 °C Freeze-drying for at least 24 h to allow the ice to sublime. During the SEM test, two spray gold treatments were performed on the TT-ES, and the better flatness was selected as the observation surface.

### Data analysis

SPSS 26.0 and Origin 2018 were used to calculate and analyze the experimental data, respectively. Particle (pore) and Cracks Analysis System (PCAS), PS, and CAD software were adopted for image processing and graphing purposes (Liu et al. 2011; Jin et al. 2016).

## Results

### The no-load expansion rate of the thermal treatment sample

Figure 3 shows a time history curve of the no-load expansion rate of the TT-ES at the different heating temperatures. When the diesel content remains the same, with increasing heating temperature, the TT-ES's no-load expansion rate decreases, and the expansion time history curve considerably changes. For example, at a diesel content of 4.0 wt%, the Steady ER of TT-ES $S_{III,1\#}$ is 25.48%, while the Steady ER of TT-ES $S_{III,2\#}$ reaches 12.6%, which is approximately 50% lower than that of TT-ES $S_{III,1\#}$. Beyond a heating temperature of 500 °C, the TT-ES expansion characteristics disappeared. The expansion time history curve of TT-ES $S_{III,1\#}$ exhibited three stages, namely, the rapid expansion stage, deceleration expansion stage, and slow expansion stage, similar to the results of Pan et al. (2020a, b). Similarly, the expansion time history curves of TT-ES $S_{III,2\#}$, $S_{III,3\#}$, $S_{III,4\#}$, and $S_{III,5\#}$ also exhibited the same three stages. However, the duration of the rapid and deceleration expansion stages was reduced. The higher the heating temperature was, the greater the reduction. Above a heating temperature of 500 °C, the expansion time history curve resembled a straight line. In addition, it should be noted that at the rapid expansion stage, the higher the heating temperature was, the higher the no-load expansion rate. For example, under a heat treatment duration of 2 h, TT-ESs $S_{III,1\#}$, $S_{III,2\#}$, $S_{III,3\#}$, and $S_{III,4\#}$ correspondingly attained no-load expansion rates of 2.20%, 2.88%, 3.54%, and 3.82%, respectively. When the heating temperature remains constant, the Steady ER decreases with increasing diesel fuel content. For example, at a heating temperature of 300 °C, the Steady ER of TT-ES $S_{I,3\#}$, $S_{II,3\#}$, $S_{III,3\#}$, and $S_{IV,3\#}$ are 16.68%, 15.00%, 9.97%, and 7.17%, respectively. The larger the diesel fuel amount is, the shorter the duration of the rapid and slow expansion stages of the time history curve.

Through data fitting of the time history curve, it is found that the fitting result agrees with the logistic function model (Zou et al. 2020). The commonly adopted expression form of the logistic function model is:

$$\delta_t = \mathrm{K}\left(1 - \frac{1}{(t/\mathrm{f})^{\mathrm{q}}}\right) \tag{1}$$

where $\delta_t$ is the corresponding no-load expansion rate at time $t$ and $K$, $f$, and $q$ are related parameters.

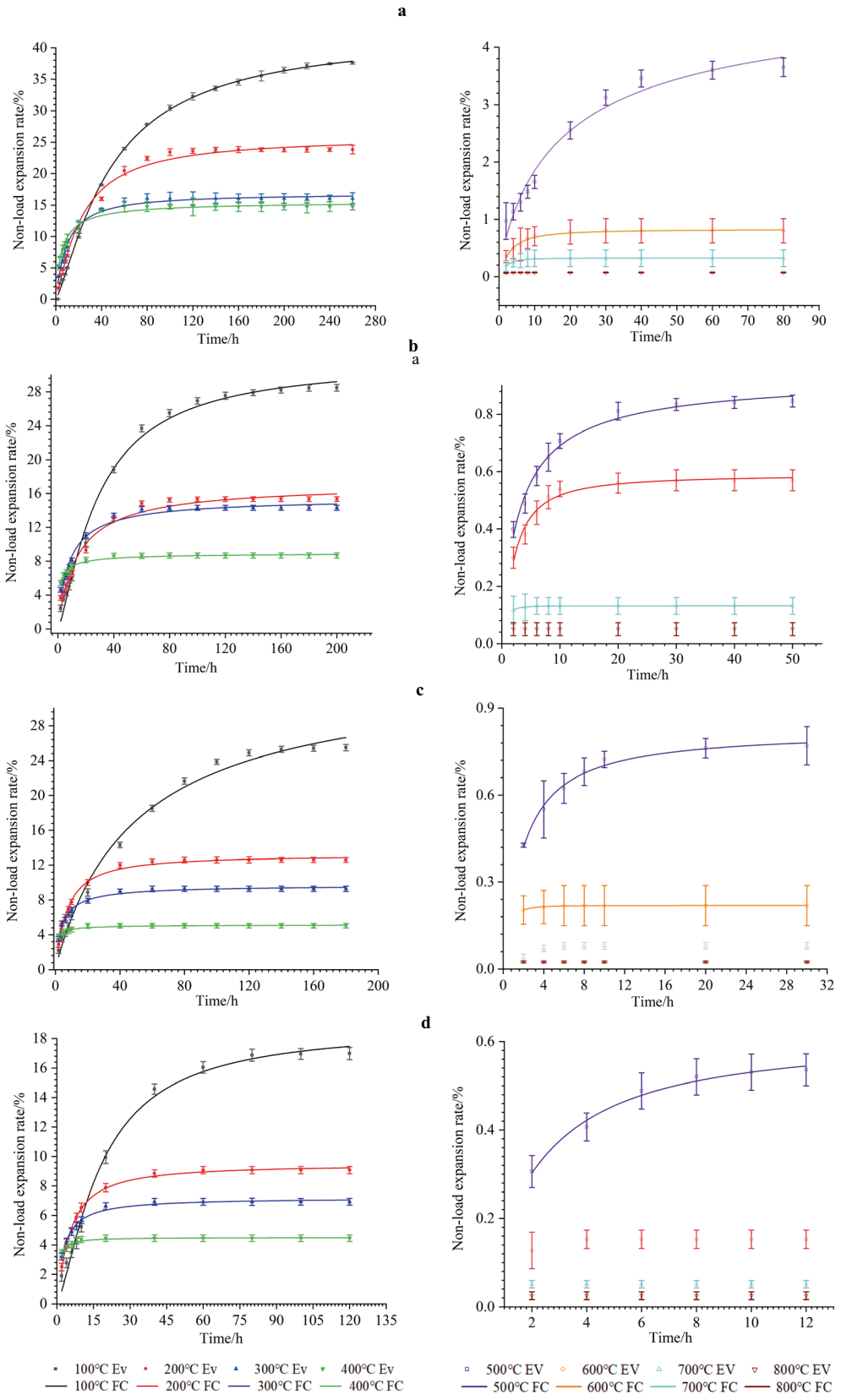


**Fig. 3** Time history curve of the no-load expansion rate of the sample. (**a**) 0.0wt%. (**b**) 2.0wt%. (**c**) 4.0wt%. (**d**) 6.0wt%. The picture is drawn with the origin and used for data fitting

**Table 2** The multivariate fitting results of time history curve of no-load expansion of the TT-ES

| Parameter | $S_{I,1\#}$ | $S_{I,2\#}$ | $S_{I,3\#}$ | $S_{I,4\#}$ | $S_{I,5\#}$ | $S_{I,6\#}$ | $S_{I,7\#}$ | $S_{I,8\#}$ | $S_{II,1\#}$ | $S_{II,2\#}$ | $S_{II,3\#}$ | $S_{II,4\#}$ | $S_{II,5\#}$ | $S_{II,6\#}$ | $S_{II,7\#}$ | $S_{II,8\#}$ |
|---|---|---|---|---|---|---|---|---|---|---|---|---|---|---|---|---|
| $K$ | 42.355 | 25.826 | 16.887 | 15.604 | 5.031 | 0.830 | 0.326 | - | 31.637 | 17.162 | 15.507 | 9.018 | 0.936 | 0.589 | 0.132 | - |
| $f$ | 48.824 | 22.079 | 9.380 | 5.411 | 19.394 | 2.790 | 1.759 | - | 29.226 | 13.895 | 7.811 | 1.236 | 3.141 | 2.092 | 0.766 | - |
| $q$ | 1.275 | 1.214 | 1.088 | 0.888 | 0.818 | 1.234 | 1.652 | - | 1.293 | 0.967 | 0.919 | 0.720 | 0.893 | 1.260 | 2.086 | - |
| $\boldsymbol{R^2}$ | 0.999 | 0.991 | 0.990 | 0.981 | 0.968 | 0.982 | 0.937 | - | 0.993 | 0.978 | 0.978 | 0.980 | 0.982 | 0.968 | 0.970 | - |
| Parameter | $S_{III,1\#}$ | $S_{III,2\#}$ | $S_{III,3\#}$ | $S_{III,4\#}$ | $S_{III,5\#}$ | $S_{III,6\#}$ | $S_{III,7\#}$ | $S_{III,8\#}$ | $S_{IV,1\#}$ | $S_{IV,2\#}$ | $S_{IV,3\#}$ | $S_{IV,4\#}$ | $S_{IV,5\#}$ | $S_{IV,6\#}$ | $S_{IV,7\#}$ | $S_{IV,8\#}$ |
| $K$ | 34.516 | 13.204 | 9.731 | 5.170 | 0.821 | 0.219 | - | - | 18.73 | 9.466 | 7.208 | 4.506 | 0.609 | - | - | - |
| $f$ | 50.866 | 6.835 | 3.730 | 0.511 | 1.918 | 0.547 | - | - | 17.96 | 5.127 | 2.693 | 0.695 | 2.031 | - | - | - |
| $q$ | 0.965 | 1.099 | 0.910 | 0.710 | 1.075 | 1.940 | - | - | 1.381 | 1.155 | 1.008 | 1.069 | 1.198 | - | - | - |
| $\boldsymbol{R^2}$ | 0.992 | 0.995 | 0.991 | 0.954 | 0.985 | 0.967 | - | - | 0.992 | 0.996 | 0.987 | 0.941 | 0.98 | - | - | - |

The fitting results are summarized in Table 2. Except for the TT-ESs corresponding to a heating temperature of 800 °C and certain TT-ESs exposed to heating temperatures of 600 and 700 °C, the expansion time history curves of the other TT-ESs are suitably fitted, and the $R^2$ values are all higher than 0.95.

Multivariate data fitting is performed on the Steady ER data of the TT-ESs, and the following relationship between the heating temperature and diesel fuel amount and the no-load expansion rate can be obtained:

$$\delta = \left(-0.5131 + 7.37e^{-0.0038x}\right)(-0.7265y + 8.164)R^2 = 0.965 \quad (2)$$

where $\delta$ is the TT-ESs no-load expansion rate under steady-state conditions.

Figure 3 shows a comparison and analysis of the Steady ER test data and fitting results. Figure 4 shows a comparison of test value and data fitting result the Steady ER of the TT-ES.

The obtained TT-ES data were subjected to a two-way analysis of variance, and the results are listed in Table 3. Two-way analysis of variance revealed that the heating temperature and diesel fuel content yielded statistically significant effects on the Steady ER of the TT-ES ($p$-value = 0 < 5%). The statistical model reflects nearly 100% of the observed variation rate. The heating temperature accounts for 85.5% of the reduction effect on the Steady ER of the TT-ES, the diesel content accounts for 7.4% of the reduction effect, and the interaction between the heating temperature and diesel content accounts for 7.1% of the reduction effect. This suggests that the heating temperature, the amount of diesel fuel, and their interaction greatly influence the reduction in the Steady ER of the TT-ES. The heating temperature reduces the Steady ER of the TT-ES more than does the diesel content, and their interaction decreases the Steady ER of the TT-ES.

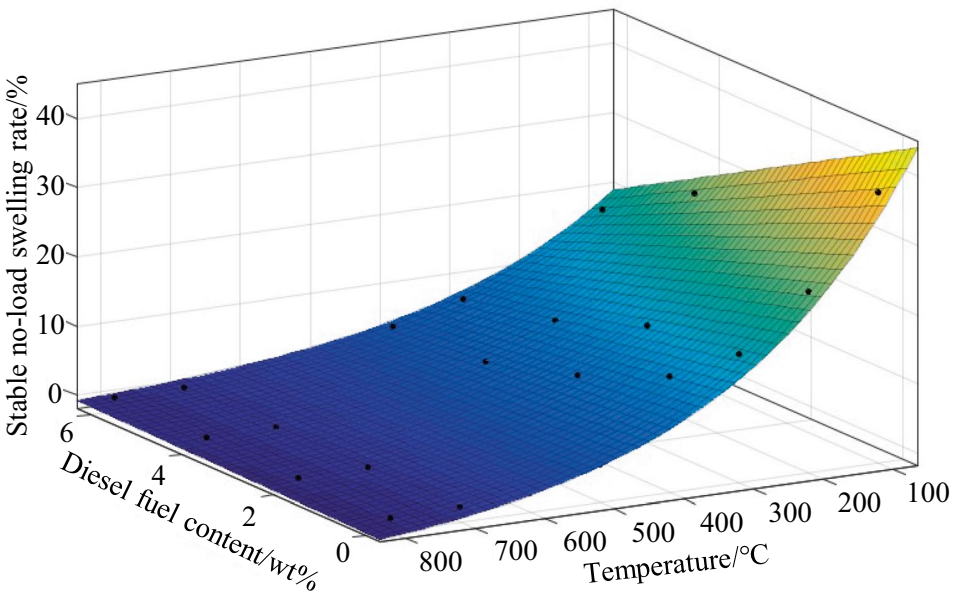


**Fig. 4** Comparison of test value and data fitting result of sample no-load expansion rate. The data is fitted by Matlab and the picture is output

**Table 3** The results of two-factor variance analysis of the no-load expansion rate of TT-ES

| Source of variation | Type III sum of squares | Df | Mean squares | *F* | *p*-value |
|---|---|---|---|---|---|
| Corrected model | 9356.058[a] | 31 | 301.808 | 26,070.595 | 0.00 |
| Intercet | 6433.382 | 1 | 6433.382 | 555,723.866 | 0.00 |
| Heating temperature | 7999.653 | 7 | 1142.808 | 98,717.200 | 0.00 |
| Diesel content | 693.025 | 3 | 231.008 | 19,954.803 | 0.00 |
| Interaction between heating temperature and diesel content | 663.380 | 21 | 31.590 | 2728.744 | 0.00 |
| Error | 0.741 | 64 | 0.012 | - | - |
| Total | 15,790.180 | 96 | - | - | - |
| Corrected total | 9356.799 | 95 | - | - | - |

*Df* degree of freedom

[a]$R^2 = 1.000$ (Corrected $R^2 = 1.000$)

## Discussion

### The effect mechanism of clay minerals on the reducing of the expansion characteristics of the thermal treatment soil

#### The effect of clay mineral content

Based on the XRD analysis results of the pollution-free background soil (0.0 wt% diesel content and a heating temperature of 100 °C), it is observed that the TT-ES expansion characteristics are attributed to the high illite content. Although illite does not experience crystal layer expansion, its surface exhibits strong hydrophilic properties, which can produce a thicker hydration layer, thus increasing the volume of clay particles and ultimately leading to an overall soil volume increase (Liu et al. 2016, 2021). Therefore, changes in the illite content inevitably cause changes in the expansion characteristics.

The TT-ESs with a diesel oil content of 4.0 wt% exposed to the different heating temperatures were analyzed. XRD results and the variation in illite and other clay minerals are shown in Fig. 5a. According to the analysis of the XRD test results, kaolinite is the most variable clay mineral, which undergoes the dehydroxylation reaction at heating temperatures ranging from 400 ~ 500 °C, resulting in the formation of metakaolin (Yan et al. 2017) and the disappearance of the corresponding strength peak in the XRD curve. Illite and quartz did not change significantly, their content remained unchanged, and their proportions varied between 37.2% and 38.5%. However, according to the research of (Escalera et al. 2014) and (Dietel et al. 2017), etc., illite gradually undergoes the dehydroxylation reaction within the temperature range from 400 ~ 800 °C, but the crystal structure of illite is still maintained in the resultant product (Wang et al. 2017). Therefore, within the temperature range from 400 to 800 °C, the XRD results reflect both illite and dehydrated illite (Jiang et al. 2008). Hence, it is not feasible to analyze the effect of the different heating temperatures on the expansion characteristics of diesel oil-contaminated soil based only on the change in the illite content measured via XRD.

Moreover, the temperature nodes before and after illite dehydroxylation are selected to analyze the effect of the diesel oil content. The selected heating temperature nodes include 300 °C and 700 °C. Figure 5b shows that illite, kaolinite, and quartz occur among all clay minerals at the four diesel oil contents. At a heating temperature of 300 °C, the illite content in TT-ESs $S_{I,3\#}$, $S_{II,3\#}$, $S_{III,3\#}$, and $S_{IV,3\#}$ is 37.2 wt%, 37.2 wt%, 36.9 wt%, and 37.0 wt%, respectively. The illite content in the $S_{I,7\#}$ and $S_{III,7\#}$ samples is 37.1 wt% and 37.7 wt%, respectively. The addition of diesel oil does not affect the physicochemical reactions of the clay minerals. Therefore, it is also impossible to analyze the effect of the diesel oil content on the expansion characteristics of the TT-ESs from the perspectives of the clay mineral composition and content.

#### The effect of the crystal structure of clay minerals

Under high temperatures, the crystal structure of clay minerals in the TT-ES will change, which affects the hydration characteristics of the TT-ESs. The main crystal interplanar spacing of illite, which affects the expansion characteristics, is analyzed at each heating temperature node. The results are shown in Table 4. The results show that the crystal structure of illite shrinks when the heating temperature is between 100 °C and 500 °C. For example, the diffraction peak plane 002 changes from 9.9465 nm to 9.8992 nm. When the heating temperature is higher than 500 °C, the illite crystal begins to expand, and the diffraction peak 002 increases from 9.8992 nm to 10.1747 nm. The results are similar to those of (Escalera et al. 2014). In the heating temperature range of 100 °C to 500 °C, during this period, the crystal structure of illite shrinks due to the loss of adsorbed water and interlayer water. But its contraction is linear and reversible. When the surface of illite regains moisture, the

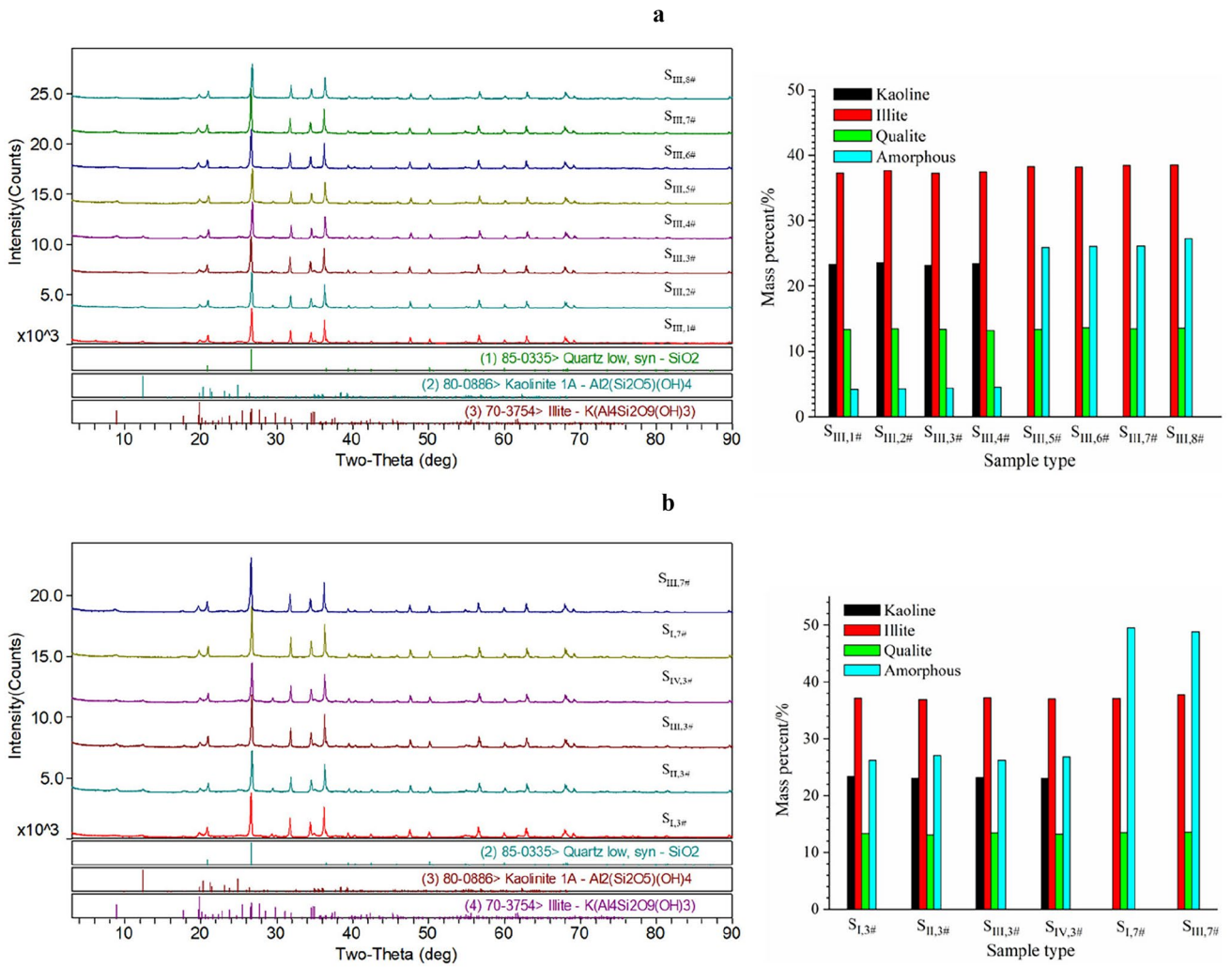


**Fig. 5** XRD analysis of samples. (**a**) The influence of different heating temperatures on clay minerals. (**b**) The influence of different diesel oil content on clay minerals. The picture is drawn with jade and origin and processed with PPT

hydration and its degree will not change, and the expansion characteristics of the sample will not change (Hueckel 2002). After the heating temperature is 500 °C, the illite is dehydroxylated and the crystal structure collapses, which is a nonlinear change. When the surface of illite regains moisture, the rehydration characteristics of dehydrated illite will be weakened (Berkelhamert 2010), which will reduce the expansion characteristics of the TT-ES.

**Table 4** Main diffraction peak (d)

| Crystal face index | TT-ES number | | | | | | | |
|---|---|---|---|---|---|---|---|---|
| | $S_{III,1\#}$ | $S_{III,2\#}$ | $S_{III,3\#}$ | $S_{III,4\#}$ | $S_{III,5\#}$ | $S_{III,6\#}$ | $S_{III,7\#}$ | $S_{III,8\#}$ |
| d(002)/nm | 9.9465 | 9.9471 | 9.9279 | 9.8812 | 9.8992 | 1.0827 | 10.1747 | 9.9278 |
| d(004)/nm | 4.979 | 4.9789 | 4.9789 | 4.9733 | 4.9572 | 5.0248 | 5.0405 | 4.9956 |
| d(-116)/nm | 2.8099 | 2.8083 | 2.8083 | 2.8016 | 2.8031 | 2.8135 | 2.8166 | 2.8032 |
| d(-133)/nm | 2.4716 | 2.4714 | 2.4712 | 2.4674 | 2.4675 | 2.4755 | 2.4768 | 2.4676 |
| d(-118)/nm | 2.2794 | 2.2784 | 2.2784 | 2.274 | 2.275 | 2.2817 | 2.2838 | 2.276 |
| d(-137)/nm | 1.9779 | 1.9778 | 1.9771 | 1.9745 | 1.9746 | 1.9797 | 1.9805 | 1.9747 |

## The effect mechanism of the cation exchange capacity on the reducing of the expansion characteristics of the thermal treatment soil

According to the theory of the electric double layer, the structure of the hydration layer on the illite surface is caused by the adsorption of water molecules by the cation exchange occurring on the crystal surface, and the cation exchange capacity determines the adsorption capacity of water molecules (Yilmaz 2004; Mehta and Sachan 2017). Figure 6a shows the cation exchange capacity in TT-ES $S_{III,1\#}$, $S_{III,2\#}$, $S_{III,3\#}$, $S_{III,4\#}$, $S_{III,5\#}$, $S_{III,6\#}$, $S_{III,7\#}$, and $S_{III,8\#}$, with a diesel oil content of 4.0 wt%. When the heating temperature varied between 100 and 400 °C, the cation exchange capacity increased to a certain extent, but the increase was limited. The cation exchange capacity increased from 33.67 c mol(+)/kg to 36.98 c mol(+)/kg. Beyond 400 °C, The cation exchange capacity is reduced to 8.93 c mol(+)/kg. This is different from the results obtained by Önal (2007). He reported that the cation exchange capacity always decreases with increasing heating temperature. The reason may be that the increase in the cation exchange capacity within the heating temperature range from 100 to 400 °C occurs due to the production of additional cation exchange capacity via organic matter pyrolysis (Marcos et al. 2007; Yan et al. 2017). After the heating temperature exceeds 400 °C, the cation exchange capacity decreases. In addition to the cause of the expansion of the illite crystal structure, it should also be related to the dehydroxylation of the kaolinite in the TT-ES to form the metakaolin. The metakaolin occurs at high temperatures, and in the cooling-induced shrinkage process, the aforementioned oxides envelop the other substances in the sample to form a eutectic, and cation exchange capacity is further incorporated into the formed eutectic (Ulery 1993; Thomaz et al. 2014), resulting in content reduction. In addition, the cation exchange capacity in TT-ESs $S_{I,3\#}$, $S_{II,3\#}$, and $S_{IV,3\#}$, were tested. The higher the diesel content was, the lower the contents of cation exchange capacity, and the decrease rate is 12.87 c mol(+)/kg. The results are shown in Fig. 6b. The reason is that after thermal desorption, the pyrolysis products of diesel oil remain in the samples and are coated on the surface of soil particles, which hinders the diffusion of exchangeable cation and reduces their content.

By comparing the change trends of the Steady ER s and the cation exchange capacity with the temperature, it is found that only part of the temperature range exhibits a positive correlation, i.e., the heating temperature range from 500 ~ 800 °C. Within this heating temperature range, the cation exchange capacity decreases, which suggests that the number of water molecule adsorption sites on the surface of clay minerals decreases, resulting in a reduction in the number of water molecules adsorbed, eventually leading to a decrease in the thickness of the surface electric double layer of clay minerals, a decline in the increase in the volume of clay particles, a reduction in the volume expansion of the whole soil, and finally a deterioration of the expansion characteristics (Prost et al. 1998). Below a heating temperature of 400 °C, the cation exchange capacity and the number of water adsorption sites did not change notably. In addition, illite shrank linearly at this stage, and its expansion characteristics did not change upon water recovery. However, the Steady ER of the TT-ES decreased with increasing heating temperature. Therefore, there should be other factors influencing the deterioration of the TT-ES expansion characteristics after thermal treatment. When the heating temperature remained constant, the higher the diesel content, the lower the cation exchange capacity was and the less notable the corresponding expansion characteristics were, which is consistent with the changing trend of the Steady ER of the TT-ES.

## The effect mechanism of the soil structure on the reducing of the expansion characteristics of the thermal treatment soil

The high-temperature environment of the thermal treatment technique can lead to the evaporation of water in the soil and

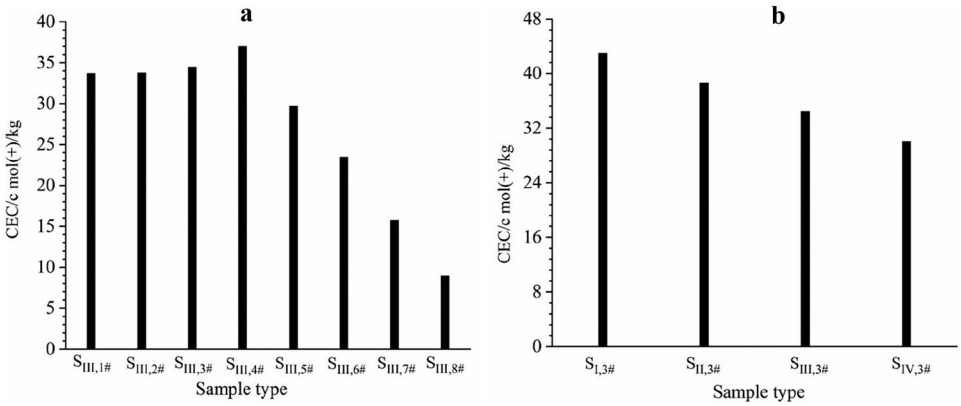


**Fig. 6** Cation exchange capacity. (**a**) The effect of different heating temperature on the content of exchangeable cation. (**b**) The effect of different diesel oil content on exchangeable cation content. The picture is drawn with the origin and processed with PPT

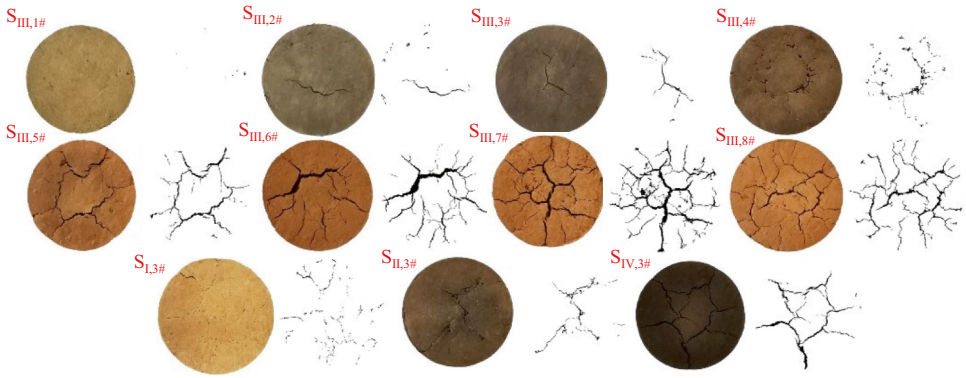


**Fig. 7** Crack diagram of a sample. The picture is processed by PCAS and processed with PPT

physical and chemical reactions of clay minerals and other soil components (O'Brien et al. 2018). This considerably alters the soil structure. For example, the samples exhibited volume shrinkage, a contact area with water was observed, a change occurred in the internal pores, and the appearance of cracks was noted. These changes affect the speed of water uptake by the TT-ESs and thus affect the TT-ES expansion characteristics. Statistics and calculations were made on the water contact area and surface cracking rate of the diesel fuel content 4.0wt%, the different heating temperature TT-ESs and the heating temperature of 300 °C, and the four diesel fuel content samples.

The area shrinkage rate and fracture rate are defined as:

$$\delta_A = 1 - \frac{S_t}{S_0} \tag{3}$$

where $\delta_A$ is the area shrinkage rate, $S_t$ is the soil area after thermal treatment, and $S_0$ is the original soil area.

$$\delta_C = \frac{S_c}{S_t} \tag{4}$$

where $\delta_C$ is the fracture rate; $S_c$ is the fracture area; and $S_t$ is the sample area after thermal treatment.

The water contact area and crack at the bottom of the TT-ES were treated by PCAS. The results are shown in Fig. 7 and Table 5. The table reveals that at a diesel oil content of 4.0 wt%, with increasing heating temperature, the larger the contact area between the TT-ES and water, the lower the area shrinkage rate and the higher the crack rate is. From TT-ES $S_{III,1\#}$ to $S_{III,8\#}$, the water contact area increased from 162,057 to 180,877 dpi, the area shrinkage rate decreased from 15.63 to 10.04%, and the crack rate increased from 0.59 to 30.62%. At a heating temperature of 300 °C, the water contact area, area shrinkage rate, and crack rate of sample $S_{I,3\#}$ are 157,440 dpi, 18.03%, and 6.4%, respectively, and the water contact area, area shrinkage rate and crack rate of $S_{IV,3\#}$ are 171,987 dpi, 10.46%, and 22.50%, respectively. With increasing diesel content, the lower the shrinkage area rate is, the larger the water contact area, and the higher the crack rate. Combined with the no-load confined expansion rate experiment results, it is determined that the larger the contact area between the TT-ES and water is,

**Table 5** List of the TT-ES structure indicators

| TT-ES number | Original TT-ES area/dpi | TT-ES area after thermal desorption/dpi | Crack area/dpi | Area shrinkage ratio/% | Cracking ratio/% | Porosity/% | Average aperture/nm |
|---|---|---|---|---|---|---|---|
| $S_{III,1\#}$ | 192,077 | 162,057 | 959 | 15.63 | 0.59 | 30.08 | 30.14 |
| $S_{III,2\#}$ | 192,077 | 164,794 | 7339 | 14.20 | 4.45 | - | - |
| $S_{III,3\#}$ | 192,077 | 164,899 | 8400 | 14.15 | 5.09 | 34.01 | 38.8 |
| $S_{III,4\#}$ | 192,077 | 170,761 | 15,079 | 11.10 | 8.83 | - | - |
| $S_{III,5\#}$ | 192,077 | 171,549 | 37,063 | 10.69 | 21.60 | 34.97 | 55.45 |
| $S_{III,6\#}$ | 192,077 | 172,787 | 46,666 | 10.04 | 27.01 | - | - |
| $S_{III,7\#}$ | 192,077 | 174,113 | 56,726 | 9.35 | 32.58 | 39.35 | 80.1 |
| $S_{III,8\#}$ | 192,077 | 180,877 | 55,383 | 5.83 | 30.62 | - | - |
| $S_{I,3\#}$ | 192,077 | 157,440 | 10,079 | 18.03 | 6.40 | 31.86 | 35.11 |
| $S_{II,3\#}$ | 192,077 | 166,757 | 26,258 | 13.18 | 15.75 | 33.21 | 36.79 |
| $S_{IV,3\#}$ | 192,077 | 171,987 | 38,693 | 10.46 | 22.50 | 39.44 | 43.22 |

the larger the amount and the higher the rate of water immersion of the soil sample per unit time, which can accelerate the hydration process of the TT-ES. However, the occurrence of surface cracks is conducive to the direct uptake of water by the TT-ES, which promotes the synchronous hydration reaction between the TT-ES and water interface. The more cracks there are the faster the water immersion process (Sobieraj et al. 2004) and the more obvious the synchronization effect. The occurrence of cracks and the increase in crack rate accelerates the hydration process of the whole TT-ES. This phenomenon is reflected in the time history curve of the no-load expansion rate of TT-ES $S_{III,1\#}$, $S_{III,2\#}$, $S_{III,3\#}$, and $S_{III,4\#}$. The higher the heating temperature at the rapid expansion stage, the higher the no-load expansion rate is.

### Effect of the internal pores

MIP experiments were carried out on TT-ES with a diesel oil content of 4.0 wt%, heating temperature of 100 °C, 300 °C, 500 °C, and 700 °C and the heating temperature of 300 °C. The test results are shown in Fig. 8 and Table 5. The test results indicate that the higher the heating temperature, the higher the porosity and average pore diameter of the TT-ES are, with increasing amounts of 9.27% and 49.96 nm, respectively. When the heating temperature remains constant, the higher the diesel content is, the higher the porosity and average pore diameter of the TT-ESs. The corresponding increase rates are 7.58% and 8.11 nm, respectively. The higher the porosity and average pore diameter, the higher the water absorption speed is, which can also accelerate the hydration process of the TT-ES. However, it is necessary to fill the sample pores before overall volume expansion occurs (Bian et al. 2019). Therefore, the larger the pore volume in the TT-ES, the more the expansion volume consumed by the hydration expansion of clay particles to fill the pores in the sample, and the contribution to the expansion of the whole sample volume will be weakened, eventually leading to the decrease of the expansion characteristics of the TT-ES. At the same time, the larger the porosity of the TT-ES, the less the content of illite in the unit volume of the TT-ES, the weaker the expansion characteristics of the TT-ES, and the lower the expansion characteristics of the TT-ES. The mechanism of the cracks produced by thermal treatment is the same as that of the pores in the specimen.

### Effect of the micro-morphology

On the one hand, the reasons for the observed shrinkage, fracturing, and changes in internal pores include the evaporation of water and an increase in matric suction (Simms and Yanful 2001). On the other hand, these phenomena are caused by physical and chemical reactions of organic matter and clay minerals (Abu-Zreig et al. 2001). XRD analysis reveals that at a heating temperature exceeding 400 °C, kaolinite undergoes a dehydroxylation reaction to produce metakaolin (Thomaz et al. 2014). The formation of these substances impacts the existing state of the other components in the TT-ESs and affects the expansion characteristics of the TT-ESs. The SEM images of TT-ESs $S_{III,1\#}$ and $S_{III,7\#}$ are compared and analyzed, as shown in Fig. 9. In Fig. 9a, a large number of irregular micron-sized flaky particles are

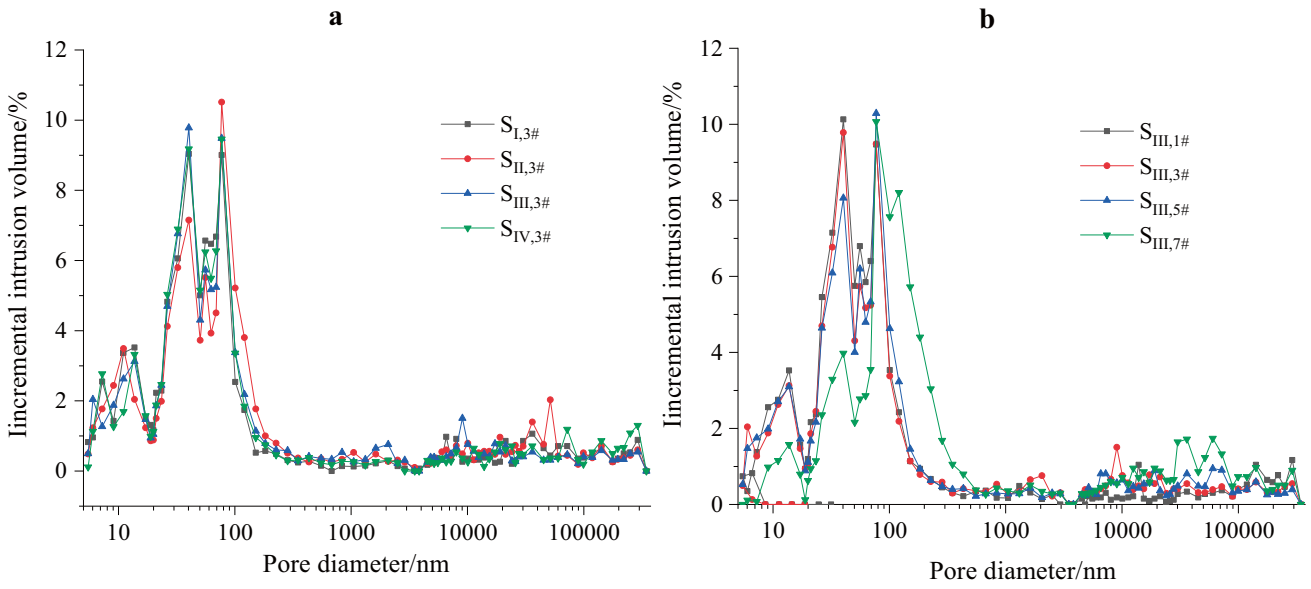


**Fig. 8** Pore distribution of samples. (**a**) The influence of different diesel oil content on pore distribution. (**b**) The influence of different heating temperatures on pore distribution. The picture is drawn with the origin and processed with PPT

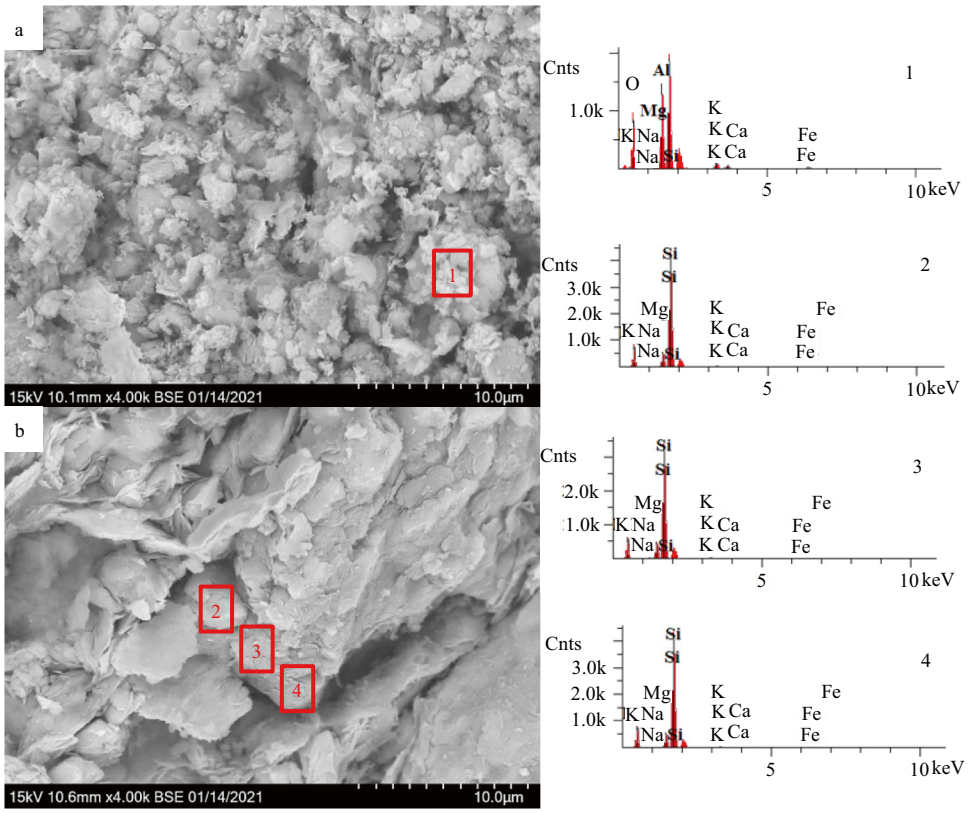


**Fig. 9** SEM picture and energy spectrum analysis of the sample. (**a**) $S_{III,1\#}$. (**b**) $S_{III,7\#}$.The picture is processed in PPT. 1: decane; 2: hendecane; 3: dodecane; 4: tridecane; 5: tetradecane; 6: pentadecane; 7: hexadecane; 8: heptadecane; 9: octadecane; 10: nonadecane; 11: eicosane; 12: n-heneicosane; 13: docosane; 14: tricosane; 15: lignocerane; 16: pentacosane; 17: hexacosane; 18: heptacosane; 19: octacosane; 20: nonacosane; 21: triacontane; 22: hentriacontane; 23: dotriacontane; 24: tritriacontane

observed, and the larger particles are assembled in a face-to-face stacking manner. The pore distribution is very compact, and the size is highly uniform. Energy spectrum analysis indicates that elements Si, Al, and K more frequently occur among the flake-shaped particles. Combined with the XRD analysis results, the flaky particles may include kaolinite and illite. As shown in Fig. 9b, a large number of small-sized flake-shaped particles disappear that is replaced by large particles generated via the melting of these small flake-shaped particles, which are assembled and stacked. Both deep and steep gullies are observed, which account for half of the whole image. According to the energy spectrum analysis results of points, 2, 3, and 4 in the figure, the K content at points 2 and 3 reaches approximately 1.33 wt% and 1.62 wt%, respectively, while the K content at point 4 is 2.70 wt%. The Si and Al contents also exhibit the same change trend at these three test points. According to the change in the element content, thermal treatment results in the mutual coating of clay minerals in the samples, which is mainly attributed to the formed metakaolin. This interaction results in the agglomeration of small particles into large particles and reduces the specific surface area, which leads to a decrease in the Steady ER (Yukselen-Aksoy and Kaya 2010). In addition, it should be noted that the resultant coating prevents the hydration reaction of clay minerals (illite) in contact with water and reduces the sample no-load expansion rate.

## The effect mechanism of the residual carbon on the reducing of the expansion characteristics of the thermal treatment soil

Thermal treatment of contaminated soil mainly includes two parts: thermal desorption and pyrolysis. Thermal desorption targets pollutants with a low molecular weight that are transformed from the liquid state into the gaseous state and are removed from soil during heating treatment. Pyrolysis involves the decomposition of pollutants with high molecular weights into other nonvolatile substances (in this paper, this indicates that alkanes containing a large number of carbon atoms are pyrolyzed into alkanes containing a small number of carbon atoms (Kang et al. 2020), which are adsorbed onto the surface of soil particles. The material remaining in the soil particles is referred to as pyrolytic carbon or coal char (Ren et al. 2020). As shown in Fig. 7, from TT-ES $S_{III,1\#}$ to sample $S_{III,8\#}$, the color changes from gray to black and finally to yellow. From TT-ES $S_{I,3\#}$ to TT-ES $S_{IV,3\#}$, the color gradually transitions from yellow to black, and the higher the content is, the higher the darkening degree. According to the color change in TT-ESs $S_{III,1\#}$, $S_{III,3\#}$, and $S_{III,5\#}$ and TT-ESs $S_{I,3\#}$, $S_{II,3\#}$, and $S_{IV,3\#}$, gas chromatography (GC-FID) experiments were conducted. The results are shown in Fig. 10. Figure 10a shows that TT-ES $S_{III,1\#}$ contains more alkanes, from decane to heptadecane containing fewer carbon atoms, and the total alkane

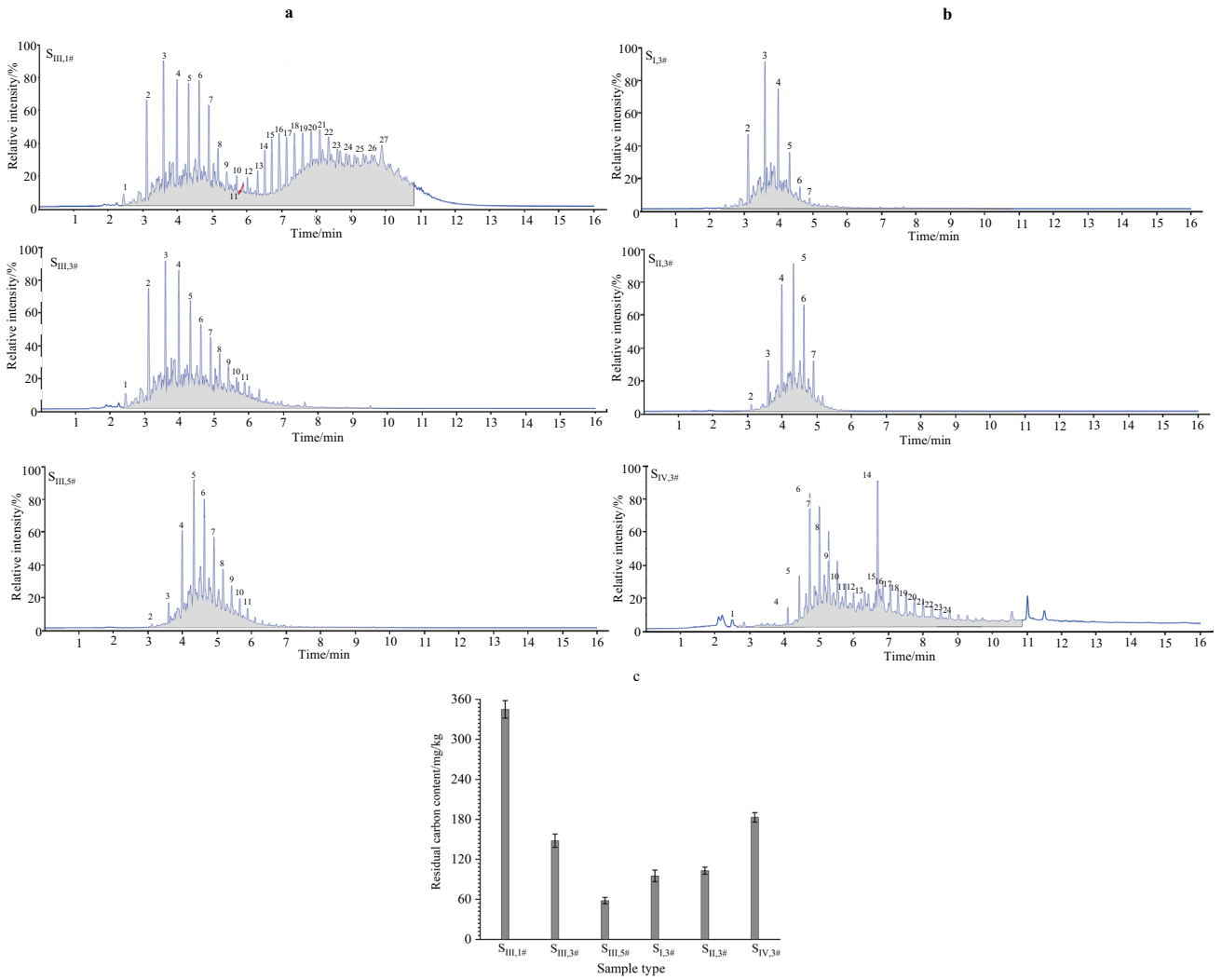


**Fig. 10** GC-FID analysis of residual carbon in samples. (**a**) The influence of different heating temperatures on residual carbon content. (**b**) The influence of different diesel fuel content on the residual carbon content. (**c**) Residual carbon content. The picture is drawn with the origin and processed with PPT

content is 345 mg/kg. The types of alkanes in sample $S_{III,3\#}$ decreases, only ranging from decane to eicosane, and the content of alkanes correspondingly decreases, with the total alkane content reaching 148 mg/kg. Although the types of alkanes in TT-ES $S_{III,5\#}$ are similar to those in TT-ES $S_{III,3\#}$, the alkane content is greatly reduced, and the total alkane content reaches 58 mg/kg. The residual carbon content in the TT-ESs decreases with increasing heating temperature. When the heating temperature remains constant, the residual carbon content in the TT-ESs increases with increasing diesel fuel content. The alkane contents in TT-ESs $S_{I,3\#}$, $S_{II,3\#}$ and $S_{IV,3\#}$ were 95, 103, and 183 mg/kg, respectively. The types of alkanes also increased with increasing diesel content.

Residual carbon is easily adsorbed and covers the surface of soil particles, thus forming a soil particle-residual carbon complex. This not only alters the interaction between soil particles and changes the pore structure of the TT-ESs but also fills the pores inside the clay particles (Zong et al. 2014). These effects inhibit contact between the soil particles and pore fluid and the hydration reaction of exchangeable cations (Pan et al. 2020a, b), thereby reducing the thickness of the electric double layer and the expansion characteristics of the TT-ESs. The higher the residual carbon content, the more obvious this weakening effect is. Therefore, the higher the diesel content, the weaker the expansion characteristics of the TT-ES. From the above research and analysis, it is observed that regarding diesel-contaminated expansive soil mainly comprising clay mineral illite, the reduction in the no-load expansion rate under heat treatment is jointly caused by several factors. These aspects include clay minerals, cation exchange capacity, soil structure, and residual carbon. When the diesel fuel amount remains unchanged, the main effect mechanism of

the reduction in the TT-ES no-load expansion rate is as follows: since XRD analysis does not distinguish between illite and dehydrated illite, the test results indicate that the illite content does not change in the entire heating temperature range. Hence, the effect mechanism cannot be explained from the perspectives of the clay mineral composition and content. However, the crystal structure expansion caused by dehydration of illite to form dehydrated illite will weaken the hydration reaction when the heating temperature is higher than 500 °C, thereby reducing the expansion characteristics of the TT-ES. The cation exchange capacity gradually decreases within the heating temperature range from 500 ~ 800 °C, which lessens the surface hydration reaction of clay particles and reduces the no-load expansion rate of the TT-ESs. The effect of the soil structure on the reduction in the sample no-load expansion rate is reflected within the full heating temperature range. The increase in the water contact area and crack rate accelerates the TT-ES hydration process and promotes the increase in the measured no-load expansion rate. As such, the no-load expansion rate at the rapid expansion stage of the TT-ES expansion time history curve varies with increasing heating temperature. The increase in the internal porosity and average pore diameter in the TT-ESs also enhances the hydration process, which yields the same effect as that of the increase in the water contact area and cracks rate. However, the ever-increasing crack rate, internal porosity, and average pore diameter eventually affect the Steady ER of the TT-ES, namely, the Steady ER is reduced. The restraining effect of the microscopic morphology change on the no-load expansion rate of the TT-ES is mainly reflected beyond a heating temperature of 400 °C. The higher the heating temperature, the lower the residual carbon content, and the weaker the contact strength between the hindered pore fluid and the clay particles, and the no-load expansion rate of the TT-ESs should be increased. However, with decreasing residual carbon content, the no-load expansion rate of the TT-ESs decreases. The effect of residual carbon on the no-load expansion rate of the TT-ESs within the study temperature range does not play a decisive role. When the heating temperature remains constant, the primary effect mechanism of the decrease in the no-load expansion rate of the TT-ESs is as follows: similarly, the analysis shows that different diesel fuel content will not affect the clay minerals, and it is not feasible to use clay minerals to analyze the impact of diesel fuel content on the reduction of the TT-ES's no-load expansion rate. The incorporation of diesel fuel can lead to a decrease in the cation exchange capacity and an increase in the water contact area, crack rate, porosity, average pore size, and residual carbon content. These effects jointly reduce the no-load expansion rate of the TT-ESs.

## Conclusions

Thermal treatment can notably reduce the expansion characteristics of diesel-polluted expansive soil. When the diesel content remains constant, the higher the heating temperature, the lower the TT-ES's Steady ER is. Moreover, the time history curve changes from a three-stage curve to a straight line. There is no change in the content of illite measured by XRD, but the change of its crystal structure has an impact on the expansion characteristics within the heating temperature range from 500 ~ 800 °C. The soil structure affects the reduction in the TT-ES's Steady ER within the full heating temperature range, while the cation exchange capacity affects the reduction in the TT-ES's Steady ER within a higher temperature range (500 ~ 800 °C). When the heating temperature remains unchanged, the larger the diesel fuel amount, the lower the TT-ES's the Steady ER is. The residual carbon produced by thermal treatment leads to changes in the cation exchange capacity of the soil and the structure of the soil; at the same time, it plays a blocking role, resulting in a decrease in the no-load expansion rate of the sample.

**Author contribution** Conceptualization, D.Z.; writing—original draft, Y.Y.C.; writing—review and editing, D.Z. and J.D.; methodology, D.Z. and Y.Y.C.; visualization, T.L.L. and Z.H.L.; investigation, J.W.Q. and J.S.; supervising, D.Z.; resources, J. S.; funding acquisition, D.Z., Z.H.L. and J.D.

**Funding** This work was supported by National Natural Science Foundation of China (Grant No.40772190, Grant No. 51378132 and Grant No. 42067045) and the Science Foundation for Distinguished Young Scholars of Guangxi (2017GXNSFBA198199) and Guangxi Communications Technical College announces the 2019 college-level research projects of natural science, philosophy, humanities and social science ( JZY2019KAZ05).

**Availability of data and materials** The datasets used and/or analyzed during the current study are available from the corresponding author on reasonable request.

## Declarations

**Ethics approval** Not applicable.

**Consent to participate** Not applicable.

**Consent for publication** Not applicable.

**Competing interests** The authors declare no competing interests.

## References

Abu-Zreig MM, Al-Akhras NM, Attom MF (2001) Influence of heat treatment on the behavior of clayey soils. Appl Clay Sci. https://doi.org/10.1016/S0169-1317(01)00066-7

Ali H, Mohamed M (2018) The effects of lime content and environmental temperature on the mechanical and hydraulic properties of extremely high plastic clays. Appl Clay Sci. https://doi.org/10.1016/j.clay.2018.04.012

Badía-Villas D, González-Pérez JA, Aznar JM, Arjona-Gracia B, Martí-Dalmau C (2014) Changes in water repellency, aggregation and organic matter of a mollic horizon burned in laboratory: soil depth affected by fire. Geoderma. https://doi.org/10.1016/j.geoderma.2013.08.038

Berkelhamert LH (2010) Rehydration study of clays. J Am Ceram Soc. https://doi.org/10.1111/j.1151-2916.1943.tb15199.x

Bian X, YuJun C, XiaoZao L (2019) Voids effect on the swelling behaviour of compacted bentonite. Géotechnique. https://doi.org/10.1680/jgeot.17.P.283

Bojnourdi S, Narani SS, Abbaspour M, Ebadi T, Hosseini S (2020) Hydro-mechanical properties of unreinforced and fiber-reinforced used motor oil (umo)-contaminated sand-bentonite mixtures. Eng Geol. https://doi.org/10.1016/j.enggeo.2020.105886

Bortey-Sam N et al (2014) Occurrence, distribution, sources and toxic potential of polycyclic aromatic hydrocarbons (PAHs) in surface soils from the Kumasi Metropolis, Ghana. Sci Total Environ. https://doi.org/10.1016/j.scitotenv.2014.07.071

Chaineau CH, Morel JL, Oudot J (1997) Phytotoxicity and plant uptake of fuel oil hydrocarbons. J Environ Qual. https://doi.org/10.2134/jeq1997.00472425002600060005x

Dietel J et al (2017) The importance of specific surface area in the geopolymerization of heated illitic clay. Appl Clay Sci. https://doi.org/10.1016/j.clay.2017.01.001

Escalera E, Tegman R, Antti M, Odén M (2014) High temperature phase evolution of bolivian kaolinitic–illitic clays heated to 1250 °c. Appl Clay Sci. https://doi.org/10.1016/j.clay.2014.07.024

Gospodarek J, Petryszak P, Kołoczek H, Rusin M (2019) The effect of soil pollution with petroleum-derived substances on porcellio scaber latr. (Crustacea, isopoda). Environ Monit Assess. https://doi.org/10.1007/s10661-018-7181-6

Gulgun Y (2011) The effects of temperature on the characteristics of kaolinite and bentonite. Sci R Essays. https://doi.org/10.5897/SRE10.727

Han G, Cui BX, Zhang XX, Li KR (2016) The effects of petroleum-contaminated soil on photosynthesis of amorpha fruticosa seedlings. Int J Environ Sci Techno. https://doi.org/10.1007/s13762-016-1071-7

Hollanders S, Adriaens R, Skibsted J, Cizer Ö, Elsen J (2016) Pozzolanic reactivity of pure calcined clays. Appl Clay Sci. https://doi.org/10.1016/j.clay.2016.08.003

Hueckel T (2002) Reactive plasticity for clays during dehydration and rehydration. Part 1: concepts and options. Int J Plasticity. https://doi.org/10.1016/S0749-6419(00)00099-1

Inbar A, Lado M, Sternberg M, Tenau H, Ben-Hur M (2014) Forest fire effects on soil chemical and physicochemical properties, infiltration, runoff, and erosion in a semiarid mediterranean region. Geoderma. https://doi.org/10.1016/j.geoderma.2014.01.015

Jiang T, Li G, Qiu G, Fan X, Huang Z (2008) Thermal activation and alkali dissolution of silicon from illite. Appl Clay Sci. https://doi.org/10.1016/j.clay.2007.08.002

Jin J et al (2016) Influence of pyrolysis temperature on properties and environmental safety of heavy metals in biochars derived from municipal sewage sludge. J Hazard Mater. https://doi.org/10.1016/j.jhazmat.2016.08.050

Kamnikar B (2001) Managing petroleum contaminated soil: department of transportation perspective. J Environ Eng (New York, N.Y.). https://doi.org/10.1061/(ASCE)0733-9372(2001)127:12(1080)

Kang C et al (2020) Pyrolytic remediation of crude oil-contaminated soil. Sci Total Environ. https://doi.org/10.1016/j.scitotenv.2020.136498

Lee JK, Park D, Kim B (1998) Remediation of petroleum-contaminated soils by fluidized thermal desorption. Waste Manage. https://doi.org/10.1016/S0956-053X(98)00135-4

Li X et al (2019) Comparison of PAH content, potential risk in vegetation, and bare soil near Daqing oil well and evaluating the effects of soil properties on PAHs. Environ Sci Pollut R. https://doi.org/10.1007/s11356-019-05720-y

Lin B, Cerato AB (2012) Prediction of expansive soil swelling based on four micro-scale properties. B Eng Geol Environ. https://doi.org/10.1007/s10064-011-0410-7

Liu C, Shi B, Zhou J, Tang C (2011) Quantification and characterization of microporosity by image processing, geometric measurement and statistical methods: application on sem images of clay materials. Appl Clay Sci. https://doi.org/10.1016/j.clay.2011.07.022

Liu J et al (2021) Experimental investigation on hydration mechanism of Sichuan shale (China). J Petroleum Sci Eng. https://doi.org/10.1016/j.petrol.2021.108421

Liu X, Zeng W, Liang L, Xiong J (2016) Experimental study on hydration damage mechanism of shale from the Longmaxi formation in southern Sichuan Basin, China. Petroleum. https://doi.org/10.1016/j.petlm.2016.01.002

Magzoub MI et al (2017) Effects of sodium carbonate addition, heat and agitation on swelling and rheological behavior of ca-bentonite colloidal dispersions. Appl Clay Sci. https://doi.org/10.1016/j.clay.2017.07.032

Marcos E, Tárrega R, Luis E (2007) Changes in a Humic Cambisol heated (100–500 °c) under laboratory conditions: the significance of heating time. Geoderma. https://doi.org/10.1016/j.geoderma.2006.11.017

Mehta B, Sachan A (2017) Effect of mineralogical properties of expansive soil on its mechanical behavior. Geotec Geol Engin. https://doi.org/10.1007/s10706-017-0289-6

Merino J, Bucalá V (2007) Effect of temperature on the release of hexadecane from soil by thermal treatment. J Hazard Mater. https://doi.org/10.1016/j.jhazmat.2006.09.050

O'Brien PL, DeSutter TM, Casey FXM, Derby NE, Wick AF (2016) Implications of using thermal desorption to remediate contaminated agricultural soil: physical characteristics and hydraulic processes. J Environ Qual. https://doi.org/10.2134/jeq2015.12.0607

O'Brien PL, DeSutter TM, Casey FXM, Khan E, Wick AF (2018) Thermal remediation alters soil properties – a review. J Environ Manage. https://doi.org/10.1016/j.jenvman.2017.11.052

Okeke CAU (2020) Engineering behaviour of lime- and waste ceramic dust-stabilized expansive soil under continuous leaching. B Eng Geol Environ. https://doi.org/10.1007/s10064-019-01648-2

Önal M (2007) Swelling and cation exchange capacity relationship for the samples obtained from a bentonite by acid activations and heat treatments. Appl Clay Sci. https://doi.org/10.1016/j.clay.2006.12.004

Pan Y, Sun J, Feng M, Liu W, Zhao L (2020a) Study on the effect of compaction work on the unloaded expansion rate of expansive soil. IOP conference series. Earth Environ Sci. https://doi.org/10.1088/1755-1315/567/1/012028

Pan Z, Garg A, Huang S, Mei G (2020b) Swelling suppression mechanism of compacted expansive soil amended with animal and plant based biochar. Waste Biomass Valori. https://doi.org/10.1007/s12649-020-01172-5

Pérez-Cadahía B et al (2007) Initial study on the effects of prestige oil on human health. Environ Int. https://doi.org/10.1016/j.envint.2006.09.006

Pérez-Cadahía B, Laffon B, Pásaro E, Méndez J (2006) Genetic damage induced by accidental environmental pollutants. Sci World J. https://doi.org/10.1100/tsw.2006.206

Pérez-Hernández I et al (2016) Growth of four tropical tree species in petroleum-contaminated soil and effects of crude oil contamination. Environ Sci Pollut R. https://doi.org/10.1007/s11356-016-7877-5

Prost R, Koutit T, Bencharaa and Huard E (1998) State and location of water adsorbed on clay minerals : consequences of the hydration and swelling-shrinkage phenomena. Clay Clay Miner. https://doi.org/10.1346/CCMN.1998.0460201

Ren J, Song X, Ding D (2020) Sustainable remediation of diesel-contaminated soil by low temperature thermal treatment: improved energy efficiency and soil reusability. Chemosphere. https://doi.org/10.1016/j.chemosphere.2019.124952

Roh Y et al (2000) Thermal-treated soil for mercury removal: soil and phytotoxicity tests. J Environ Qual. https://doi.org/10.2134/jeq2000.00472425002900020007x

Simms PH, Yanful EK (2001) Measurement and estimation of pore shrinkage and pore distribution in a clayey till during soil-water characteristic curve tests. Can Geotech J. https://doi.org/10.1139/cgj-38-4-741

Sobieraj JA, Elsenbeer H, Cameron G (2004) Scale dependency in spatial patterns of saturated hydraulic conductivity. CATENA. https://doi.org/10.1016/S0341-8162(03)00090-0

Sun H, Qin X, Yang X, Zhao Y (2020) Study on the heat transfer in different aquifer media with different groundwater velocities during thermal conductive heating. Environ Sci Pollut R. https://doi.org/10.1007/s11356-020-09131-2

Thomaz et al (2014) Effects of fire on the physicochemical properties of soil in aslash-and-burn agriculture. CATENA. https://doi.org/10.1016/j.catena.2014.06.016

Ulery AL (1993) Forest fire effect on soil color and texture. Soil Sci Soc Am J. https://doi.org/10.2136/sssaj1993.03615995005700010026x

Vidonish JE, Zygourakis K, Masiello CA, Sabadell G, Alvarez PJJ (2016) Thermal treatment of hydrocarbon-impacted soils: a review of technology innovation for sustainable remediation. Engin. https://doi.org/10.1016/J.ENG.2016.04.005

Wang G, Huang Y, Li R, Chang J, Fu J (2020) Influence of vetiver root system on mechanical performance of expansive soil: experimental studies. Adv Civ Eng. https://doi.org/10.1155/2020/2027172

Wang G, Wang H, Zhang N (2017) In situ high temperature x-ray diffraction study of illite. Appl Clay Sci. https://doi.org/10.1016/j.clay.2017.06.006

Watabe Y, Yamada K and Saitoh K (2011) Hydraulic conductivity and compressibility of mixtures of Nagoya clay with sand or bentonite. Géotechnique. https://doi.org/10.1680/geot.8.P.087

Wei Y, Wang L (2020) Pollution characteristics and comprehensive evaluation of soil organic compounds at a chemical contaminated site. IOP conference series. Earth Environ Sci. https://doi.org/10.1088/1755-1315/514/3/032045

Xiong D, Wang C (2021) Risk assessment of human exposure to heavy metals, polycyclic aromatic hydrocarbons, and radionuclides in oil-based drilling cutting residues used for roadbed materials in Chongqing, china. Environ Sci Pollut R. https://doi.org/10.1007/s11356-021-13871-0

Yan K et al (2017) Decomposition and phase transformation mechanism of kaolinite calcined with sodium carbonate. Appl Clay Sci. https://doi.org/10.1016/j.clay.2017.07.010

Yilmaz I (2004) Relationships between liquid limit, cation exchange capacity, and swelling potentials of clayey soils. Eur Soil Sci. https://doi.org/10.1081/css-120037558

Yukselen-Aksoy Y, Kaya A (2010) Predicting soil swelling behaviour from specific surface area. Proceedings of the Institution of Civil Engineers - Geotechnical Engineering. https://doi.org/10.1680/geng.2010.163.4.229

Zhang J et al (2012) Distribution and sources of petroleum-hydrocarbon in soil profiles of the Hunpu wastewater-irrigated area. China's Northeast Geoderma. https://doi.org/10.1016/j.geoderma.2011.12.004

Zong Y, Chen D, Lu S (2014) Impact of biochars on swell-shrinkage behavior, mechanical strength, and surface cracking of clayey soil. J Plant Nutr Soil Sci. https://doi.org/10.1002/jpln.201300596

Zou WL, Ye YX, Han Z (2020) Chemical reaction kinetics based models for describing evolution of one-dimensional expansion with time. Chin J Geotech Eng (in chinese). https://doi.org/10.11779/CJGE202004017